Piezoreflectivity of the Noble Metals*

M. Garfinkel, J. J. Tiemann, and W. E. Engeler

General Electric Research and Development Center, Schenectady, New York

(Received 21 March 1966)

The piezoreflectance spectra of evaporated films of copper, silver, and gold have been measured in the range 1.5–5.0 eV. The experimental results were subjected to a Kramers-Kronig analysis in order to determine the corresponding phase changes $\Delta\theta$. In this manner a complete specification of the optical properties of the strained material is made. The conditions which must be fulfilled if this Kramers-Kronig inversion is to be made are discussed. The strain-induced changes in the real and imaginary parts of the dielectric constant tensor are found to be quite similar for all three materials. The over-all structure shows qualitative agreement with the deformation-potential model, and the signs of the deformation potentials of some of the transitions are tentatively assigned. The results for all three metals show additional structure in a region lower in energy than that for which structure has been previously detected. The most reasonable explanation for this is that there are interband transitions possible at lower energy than has previously been presumed. The similarity of this structure in $\Delta\epsilon_2$ for all three metals indicates that the same transitions are involved for copper, silver, and gold.

I. INTRODUCTION

THIS paper presents some experimental measurements of the piezoreflectivity of thin films of the noble metals. Since the data do not directly yield the changes in the fundamental optical constants of the samples due to strain, these measurements must be interpreted before they can be made to yield information about the band structure and the deformation potentials of the samples. The method that was used for analyzing the data is therefore also presented in detail. Measurements of piezoreflectivity have been previously used to obtain information about band structure of solids, and their usefulness in this regard is well known. The previous methods were based on static measurements of the unstrained material and the strained material, and the changes due to stress were obtained by direct subtraction of the two curves. This technique suffers from severe experimental limitations which can be traced to fluctuations in the over-all sensitivity of the optical system.

The present experiment falls within a class of differential optical measurements which do not rely on the long term stability of the optical system. The basic approach which these experiments have in common is that the optical properties of the solid are modulated at some relatively high frequency by the periodic variation of some external parameter. These experiments include the electroreflectance studies of Seraphin et al.,[1-4] and of Shaklee et al.,[5,6] the electrotransmission

experiments of Moss,[7] of Chester and Wendland,[8,9] of Frova and Handler,[10-12] and of Yacoby,[13] the piezoreflectance measurements of Engeler et al.[14,15] and of Gobeli and Kane,[16] and the piezotransmission measurements of Engeler et al.[17] In these experiments the band structure of the solid is modulated by means of an externally applied ac field (electric field or strain field) and the resulting changes in the optical properties are detected synchronously. The electric field experiments may be performed on insulators and semiconductors and the strain experiments may be performed on metal as well. These differential experiments possess several virtues. First, because of the derivative nature of the experiments any structure in the optical properties of the material is enhanced, enabling one to locate critical-point energies more precisely and perhaps to identify new ones. Second, since the piezoreflectance effect is due to the modulation of the band structure by the applied strain, the strain experiments can give information about the deformation potentials of the various energy bands. Third, and perhaps most important, is the fact that experiments which use strain are capable of yielding information about the locations in the brillouin zone[18,19] of the interband transitions which give rise to the optical properties of the solid.

* A preliminary account of this work was given at the October 1965 meeting of the American Physical Society at Chicago [Bull. Am. Phys. Soc. **10**, 1085 (1965)].

[1] B. O. Seraphin and R. B. Hess, Phys. Rev. Letters **14**, 138 (1965).

[2] B. O. Seraphin, R. B. Hess, and N. Bottka, J. Appl. Phys. **36**, 2242 (1965).

[3] B. O. Seraphin and N. Bottka, Phys. Rev. **139**, A560 (1965); **140**, A1716 (1965).

[4] B. O. Seraphin and N. Bottka, Phys. Rev. Letters **15**, 104 (1965).

[5] K. L. Shaklee, F. H. Pollak, and M. Cardona, Phys. Rev. Letters **15**, 883 (1965).

[6] K. L. Shaklee, M. Cardona, and F. H. Pollak, Phys. Rev. Letters **16**, 48 (1966).

[7] T. S. Moss, J. Appl. Phys., Suppl. **32**, 2136 (1961).

[8] M. Chester and P. H. Wendland, Phys. Rev. Letters **13**, 193 (1964).

[9] P. H. Wendland and M. Chester, Phys. Rev. **140**, A1384 (1965).

[10] A. Frova and P. Handler, Appl. Phys. Letters **5**, 11 (1964).

[11] A. Frova and P. Handler, Phys. Rev. **137**, A1857 (1965).

[12] A. Frova and P. Handler, Phys. Rev. Letters **13**, 193 (1964).

[13] Y. Yacoby, Phys. Rev. **142**, 445 (1966).

[14] W. E. Engeler, H. Fritzsche, M. Garfinkel, and J. J. Tiemann, Phys. Rev. Letters **14**, 1605 (1965).

[15] W. E. Engeler, M. Garfinkel, J. J. Tiemann, and H. Fritzsche, in *Proceedings of the International Colloquium on Optical Properties and Electronic Structure of Metals and Alloys, Paris, 1965* (North-Holland Publishing Company, Amsterdam, 1966).

[16] G. W. Gobeli and E. O. Kane, Phys. Rev. Letters **15**, 142 (1965).

[17] W. E. Engeler, M. Garfinkel, and J. J. Tiemann, Phys. Rev. Letters **16**, 239 (1966).

[18] U. Gerhardt, Phys. Rev. Letters **15**, 401 (1965).

[19] U. Gerhardt, Phys. Status Solidi **11**, 801 (1965).

In Sec. II we present the experimental details that are relevant to this experiment. Section III contains a discussion of the conditions that are necessary for meaningful $\Delta R/R$ measurements to be made. Section IV gives a procedure for treating the $\Delta R/R$ data in order to obtain $\Delta\epsilon_2$, the strain-induced change in the imaginary part of the dielectric constant. Methods of extrapolating the data to higher and lower energies are discussed. In Sec. V we present and discuss the experimental results. The experimental results for Cu^{14} and a brief outline of parts of Sec. IV have been presented previously,[15] but we include them in the interest of completeness.

II. EXPERIMENTAL

A schematic view of the experimental apparatus is shown in Fig. 1. The measurements were all made at room temperature using unpolarized light at near-normal incidence. The light beam whose wavelength was swept by the monochromator was incident upon a sample of the material under investigation. The sample itself consisted of a 1-μ film of the metal which had been evaporated directly upon the polished face of a piezo-electric transducer of the lead zirconate titanate type. The transducer was driven by an ac voltage, and its deformation strained the film. The reflected beam thus contained a modulated component. This beam fell upon the photodetector and the output of this detector was split into an ac and a dc component. The dc component depends upon the reflectivity R of the unstrained material. The ac component was measured synchronously with the applied oscillatory strain by means of the lock-in amplifier shown. This ac component is proportional to the changes in the reflectivity ΔR which are due to the strain-induced changes in the optical constants of the material. Since the analysis requires only the ratio $\Delta R/R$, the absolute values of these signals is not important.

The ratio $\Delta R/R$ was obtained in several different ways, and this quantity was recorded directly. One method used was to keep the dc component of the reflectivity signal constant by controlling the gain of the photodetector itself. If the dc component is constrained to be constant, then the ac component is proportional to $\Delta R/R$ as desired. Another method used was to run the photodetector at constant gain and take the ratio $\Delta R/R$ electronically. This mode of operation requires that the detector be linear over a sufficiently wide range. In the range of photon energy above 2.0 eV a photomultiplier having the S11 response was used. In the range below 2.1 eV, a silicon photovoltaic cell was used. In addition, some measurements were made with a lead-sulfide photodetector, but these measurements were not as satisfactory as were those made with the other two detectors. This was probably due to the small size and nonuniform sensitivity of the active area of this detector.
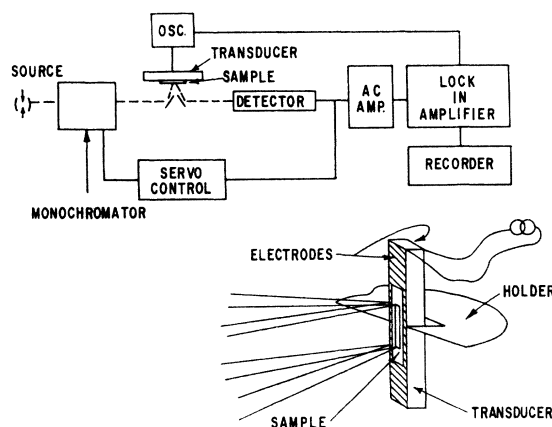
FIG. 1. Schematic view of experimental arrangement.

The metals studied were copper, silver, and gold. The films were evaporated quickly (less than 20 sec deposition time) and the substrates were kept at room temperature. Diffractometer studies indicated that the films were composed of crystallites having either a $\langle 111 \rangle$ or a $\langle 100 \rangle$ axis normal to the plane of the film and being otherwise randomly oriented. Subsequent to their evaporation the samples were stored in a nitrogen filled desiccator until they were used. The results for gold showed no changes between measurements made "immediately" after evaporation (within the first day of exposure to air). Copper samples, however, when exposed to air for one week, exhibited an approximately 25–50% decrease in $\Delta R/R$ in the range of photon energy just above 2 V.

A high-pressure xenon arc lamp was used in obtaining the data over the entire wavelength range. Special care was taken to filter the power supply for the arc lamp, since the response time of the arc is much shorter than one cycle of the 1-kc operating frequency. In order to reduce spurious signals due to mechanical vibrations of both the photomultiplier and the Si photodetector, it was necessary to mount the transducer in such a way that its center of mass remained essentially at rest. In addition, it was necessary to mechanically decouple the photomultiplier from the oscillating sample in order to eliminate a false signal due to mechanical motion of the dynode structure.

In order to obtain the ratio $\Delta R/R$ correctly, it is necessary that the gain of the dc component and the ac component be calibrated with respect to each other. In order to obtain a good noise figure, it was desirable to run the ac amplifier with the highest possible input impedance. This high impedance together with the output capacitance of the photodetector caused a significant difference in the gain of the ac channel with respect to the dc channel. This difference was calculated from the measured values of input resistance and capacitance and was checked by means of a gallium phosphide light emitting diode with known ac and dc

components in its light output. The calculated drop-off in gain of the ac signal agreed with the experimental calibration within 1%. There were several lines in the spectral output of the xenon lamp that was used which were sufficiently sharp to cause transients that were comparable to the response time of the recording system. In order to prevent these transients from introducing spurious structure in the output plots, the transient response of the ΔR channel was adjusted so that it was equal to the transient response of the R channel. When this was done, sudden changes in light intensity produced little or no effect on the recorded data.

As was mentioned by us[14] and by Gobeli and Kane[16] the zero of the measured values of $\Delta R/R$ is uncertain because of a wavelength- independent error signal which is difficult to avoid. There are several origins of this spurious signal. First, since the light beam falling upon the sample is not perfectly homogeneous and is finite in size, any imperfection in the vibrating sample surface modulates the reflected light intensity at the same frequency as the true signal. Second, the presence of any imperfection in the optical path after the light has been reflected from the sample or any nonuniformity of the detector sensitivity will cause some intensity modulation through the slight, unavoidable, lateral vibrations of the light beam coherent with the excitation.

The effect of the first source of zero offset was minimized by placing the sample at a point where the beam aperture was slightly out of focus, and by keeping the slits at a constant setting. The second source of zero offset was minimized by placing the monochromator ahead of the sample rather than behind it. In this way, the slits of the monochromator do not convert the lateral deviation to an amplitude modulation, and, in addition, the stray light is unmodulated. The true zero level of $\Delta R/R$ may be determined by an analytical procedure that will be described below. For the data above 2.0 eV, the photomultiplier gain was continuously varied to keep the R signal constant. For the data below 2.1 eV, the ratio of the ΔR and the R signal was taken electronically.

III. PIEZO-OPTICAL EFFECTS IN CUBIC CRYSTALS

A review of the effects of strain upon the optical properties of cubic crystals is useful in understanding the data reduction process. In addition, it is desirable to define precisely the necessary conditions that must be present for the analysis to work.

Since a knowledge of the dielectric constant is sufficient to describe the optical properties of the solid, it is possible to completely describe the piezo-optic interaction in terms of the changes in the dielectric constant induced by strain. There exists a complete set of experiments for which the analysis presented below is valid and from which a complete knowledge of the changes

in the optical constants caused by strain can be deduced. As in the case of the present experiments, however, it is sometimes not convenient to obtain the single-crystal specimens that are needed to perform this complete set of experiments. In such a case, it is desirable to know what can be obtained and what cannot be obtained from a smaller number of experiments.

The dielectric constant ϵ connects the charge displacement vector D and the electric-field vector E. Since both D and E are polar vectors ϵ is a second-rank tensor. Since the polarization vector is not necessarily in phase with the electric field, the dielectric constant must be complex. It can therefore be expressed as $\epsilon = \epsilon_1 + i\epsilon_2$, where ϵ_1 and ϵ_2 are both real second-rank tensors. The state of strain of a body e is also described by a second-rank tensor. Therefore the relationship between it and ϵ is given by[16,20]

$$\Delta\epsilon_{ij} = W_{ijkl}e_{kl}, \tag{1}$$

where $\Delta\epsilon_{ij}$ is the strain-induced change in ϵ, and **W** is a fourth-rank tensor.

The strain tensor is real and since the change in ϵ, $\Delta\epsilon$, is in general complex, **W** must be decomposed into two components, $\mathbf{W_1} + i\mathbf{W_2}$. Neglecting optical activity, both ϵ and e are symmetric and $\mathbf{W_1}$ and $\mathbf{W_2}$ are real symmetric fourth-rank tensors. For cubic materials in general each of the tensors $\mathbf{W_1}$ and $\mathbf{W_2}$ can be expressed in terms of four independent constants. For crystals of ($m3m$) symmetry, there are only three independent constants for each of the two tensors. In agreement with the usual convention[21,22] for fourth-rank tensors in cubic symmetry, these components are $(W_1)_{11}$, $(W_2)_{11}$, $(W_1)_{12}$, $(W_2)_{12}$, $(W_1)_{44}$, and $(W_2)_{44}$ referred to the cube axes. Thus, since the optical properties are completely specified by ϵ and $\Delta\epsilon$, these six independent constants completely specify the piezo-optical interaction for materials satisfying symmetry requirements stated above. These optical constants may be obtained from reflectivity measurements made at normal incidence. If we specify that the experiment be performed in this manner, with linear polarization and without the use of ellipsometry to analyze the reflected beam, there are several conditions which must be fulfilled. The reflected beam must remain linearly polarized and the direction of the polarization must be the same as that of the incident beam. In order for this to be true, the polarization vector of the incident beam

---

[20] J. F. Nye, *Physical Properties of Crystals* (Oxford University Press, London, 1957), p. 249 ff.

[21] J. F. Nye, *Physical Properties of Crystals* (Oxford University Press, London, 1957), p. 253.

[22] In this notation the dielectric constant and strain tensors are represented by six-component vectors and **W** becomes a 6×6 matrix. Equation (1) is then written $\Delta\epsilon_i + W_{ij}e_j$, where i and j run from 1–6. In this equation, the first three diagonal components of the strain are given by $e_j = e_{jj}$ and the last three, off diagonal, components are $e_4 = e_{23}$, etc. The three diagonal elements of the $\Delta\boldsymbol{\varepsilon}$ tensor are $\Delta\epsilon_{ii} = \Delta\epsilon_i$. However, the off-diagonal elements are related to the 4th, 5th, and 6th components of the $\Delta\boldsymbol{\varepsilon}$ six-vectors by $\Delta\epsilon_{23} = \frac{1}{2}\Delta\epsilon_4$, $\Delta\epsilon_{13} = \frac{1}{2}\Delta\epsilon_5$, and $\Delta\epsilon_{12} = \frac{1}{2}\Delta\epsilon_6$.

must be chosen along a principal axis of the material under study, and the material must not be optically active. In the case of piezoreflectivity, these conditions must be true not only for the unstrained case but must remain true for the strained case as well. For the unstrained case the first condition is automatically fulfilled for normal incidence, since unstrained cubic materials have isotropic optical properties. Under conditions of uniaxial strain, however, only certain combinations of strain direction and polarization direction are analyzable. In general, the only applied stresses which can be permitted are those which cause the index to distort from a sphere to an ellipsoid whose principal axes are fixed by symmetry, and are not, therefore, functions of wavelength nor dependent upon the magnitude of the applied stress. For more complex crystal structures, both the stressed and unstressed index ellipsoids must have the same principal axes and the light polarization must be along one of these principal directions. The requirement that neither the unstressed nor the stressed crystal be optically active excludes from the analysis changes in the optical properties due to some types of "stress" such as magnetic field.

A uniform expansion of the crystal lattice under hydrostatic pressure does not change the symmetry of the crystal. For cubic crystals, therefore, any orientation and any direction of polarization forms a valid experiment. There is only a single complex strain optical constant, however, that may be obtained in this manner. This constant is $W_{11}+2W_{12}$.

For a uniform expansion in a plane, with the expansion occurring in either a $\langle 100 \rangle$ or a $\langle 111 \rangle$ plane, the above conditions are fulfilled for any polarization vector lying in the plane of the expansion. For planes of lower symmetry the situation is more complex. Even though there is spherical symmetry for the unstrained case, the strain-induced changes are not generally independent of the angle that the polarization makes in the plane, for the two principal axes are not in general equivalent. Furthermore, they do not in general lie in the plane of the expansion. If, for example, the reflection plane consists of a random array of crystallites of $\langle 110 \rangle$ orientation, each crystallite would reflect a linearly polarized incident beam with a different amount of ellipticity. However, two of the principal axes for both the $\langle 100 \rangle$ and the $\langle 111 \rangle$ planar expansion lie in these planes and are, in addition, equivalent. Therefore, all polarization directions in these planes are equivalent and no ellipticity is imparted by the strain to the reflected beam regardless of its polarization. Reflectivity measurements made upon uniformly expanded partially oriented films of these types are thus analyzable. Two combinations of the three complex W's may be obtained. The $\langle 111 \rangle$ sample yields the results

$$\Delta\epsilon = \frac{2(S_{11}+2S_{12})(W_{11}+2W_{12})+\frac{1}{2}S_{44}W_{44}}{2(S_{11}+2S_{12})+\frac{1}{2}S_{44}}e, \qquad (2)$$

and the 100 sample gives

$$\Delta\epsilon = \left[(W_{11}+2W_{12})+\frac{S_{12}-S_{11}}{S_{11}+S_{12}}W_{12} \right]e, \qquad (3)$$

where e is the magnitude of the uniform planar expansion and S_{11}, S_{12}, and S_{44} are the usual elastic compliances.

For the case of uniaxial strain it is possible to determine the complete set of strain-optical constants if the strain and polarization are directed along properly chosen crystallographic directions. For example, with normal incidence onto a $\langle 100 \rangle$ face, uniaxial tension normal to the beam, and the polarization chosen to be either along the direction of the tension or perpendicular to it, two samples are sufficient. One sample has the tension T applied along the $\langle 010 \rangle$ direction and the other is stressed along the $\langle 011 \rangle$ axis. The expressions for the changes in ϵ for these two cases are

$$\langle 010 \rangle: \quad \Delta\epsilon_{\parallel}=[S_{11}W_{11}+2s_{12}W_{12}]T, \qquad (4)$$

$$\Delta\epsilon_{\perp}=[s_{12}W_{11}+(S_{11}+S_{12})W_{12}]T; \qquad (5)$$

$$\langle 011 \rangle: \quad \Delta\epsilon_{\parallel}=\frac{1}{2}[(s_{11}+s_{12})W_{11}$$
$$+(s_{11}+3s_{12})W_{12}+\frac{1}{2}s_{44}W_{44}]T, \qquad (6)$$

$$\Delta\epsilon_{\perp}=\frac{1}{2}[(s_{11}+s_{12})W_{11}$$
$$+(s_{11}+3s_{12})W_{12}-\frac{1}{2}s_{44}W_{44}]T. \qquad (7)$$

In Eqs. (4) and (5) the stress T is in the $\langle 010 \rangle$ direction and the polarization directions are parallel and perpendicular to it, respectively, and in Eqs. (6) and (7) the stress direction is $\langle 011 \rangle$ and the polarization directions are again parallel and perpendicular to the stress axis. These equations may be rewritten in terms of the strain e in the direction of the stress axis:

$$\langle 010 \rangle:$$

$$\Delta\epsilon_{\parallel}=[W_{11}+2(s_{12}/s_{11})W_{12}]e, \qquad (4')$$

$$\Delta\epsilon_{\perp}=\left[\frac{s_{12}}{s_{11}}W_{11}+\left(1+\frac{s_{12}}{s_{11}}\right)W_{12}\right]e; \qquad (5')$$

$$\langle 011 \rangle:$$

$$\Delta\epsilon_{\parallel}=\frac{(s_{11}+s_{12})W_{11}+(s_{11}+3s_{12})W_{12}+\frac{1}{2}s_{44}W_{44}}{S_{11}+S_{12}+\frac{1}{2}S_{44}}e, \qquad (6')$$

$$\Delta\epsilon_{\perp}=\frac{(s_{11}+s_{12})W_{11}+(s_{11}+3s_{12})W_{12}-\frac{1}{2}s_{44}W_{44}}{s_{11}+s_{12}+\frac{1}{2}s_{44}}e. \qquad (7')$$

IV. PROCEDURE FOR TREATING THE DATA

This section presents a method for reducing the experimentally measured values of $\Delta R/R$ to the more meaningful quantities $\Delta\epsilon_1$ and $\Delta\epsilon_2$. Just as the state of unperturbed crystal requires both ϵ_1 and ϵ_2 for its specification, the perturbed crystal requires a knowledge of ϵ_1, ϵ_2, $\Delta\epsilon_1$, $\Delta\epsilon_2$ for its full description. The differential-

reflectance measurements themselves $\Delta R/R$ together with ϵ_1 and ϵ_2 are thus not sufficient. If, however, the change in phase of the reflected light $\Delta\theta$ is also known, then this, together with a knowledge of $\Delta R/R$, R, and θ, is sufficient to uniquely specify the changes in the dielectric constant at the wavelength involved. It is well known that the real and imaginary parts of the dielectric constant are not completely independent. If one of these functions is completely specified as a function of frequency, the other one is completely determined by the Kramers-Kronig relationship.[23] Since this statement is equally true for both the unstrained case and the strained case, it follows that the changes in the dielectric constant induced by strain also must satisfy a Kramers-Kronig relationship. This relationship may be derived directly from the usual Kramers-Kronig relation between the phase angle of the reflected wave and the reflectivity of the material.

In the usual fashion[23] this is written

$$\theta = \frac{1}{2\pi}\int_0^\infty \frac{d}{d\omega}(\ln R)\,\ln\left|\frac{\omega+\omega_0}{\omega-\omega_0}\right|d\omega, \tag{8}$$

where $r = |r|\,e^{i\theta}$ is the complex reflection coefficient and $R = |r|^2$. For the strained material under the conditions specified in Sec. III,

$$\theta+\Delta\theta = \frac{1}{2\pi}\int_0^\infty \frac{d}{d\omega}(\ln(R+\Delta R))\,\ln\left|\frac{\omega+\omega_0}{\omega-\omega_0}\right|d\omega. \tag{9}$$

Subtracting Eq. (9) from Eq. (8) yields the desired relationship,

$$\Delta\theta = \frac{1}{2\pi}\int_0^\infty \frac{d}{d\omega}\left(\frac{\Delta R}{R}\right)\ln\left|\frac{\omega+\omega_0}{\omega-\omega_0}\right|d\omega. \tag{10}$$

Thus, although the experiments do not measure $\Delta\theta$ directly, it is possible by means of Eq. (10) to relate $\Delta\theta$ at a particular wavelength to an integral of $\Delta R/R$ over all wavelengths.

If $\Delta R/R$ is known over only a limited wavelength range, the derived $\Delta\theta$ may depend very strongly on the way $\Delta R/R$ is assumed to vary outside it. If the wavelength range is sufficiently broad, however, so that the derived $\Delta\theta$ no longer depends sensitively on $\Delta R/R$ outside of it, then $\Delta\theta$ can be considered as determined by the data, and a meaningful comparison with theory can be made. The width of the region over which $\Delta R/R$ must be known depends strongly on how much structure exists outside of it, and each case must be considered on its merits.

With both $\Delta R/R$ and $\Delta\theta$ known it is possible to obtain the changes in the real and imaginary parts of the principal values of the dielectric constants. Straight-
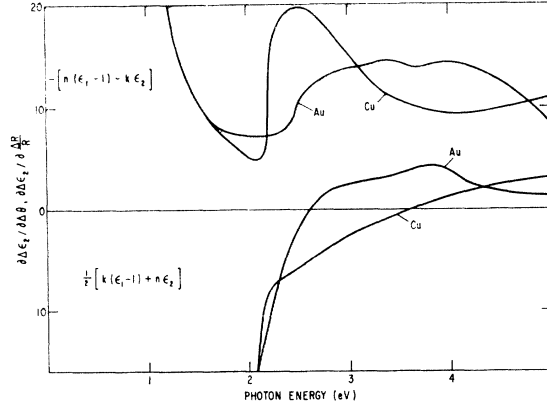
FIG. 2. The coefficients multiplying $\Delta R/R$ and $\Delta\theta$ in Eq. (4) evaluated for copper and gold. The quantity $-[n(\epsilon_1-1)-k\epsilon_2]$ multiplies $\Delta\theta$ and $\frac{1}{2}[k(\epsilon_1-1)+n\epsilon_2]$ multiplies $\Delta R/R$.

forward manipulation of the relations between the various sets of optical constants yields

$$\Delta\epsilon_1 = \tfrac{1}{2}[n(\epsilon_1-1)-k\epsilon_2](\Delta R/R)$$
$$+[k(\epsilon_1-1)+n\epsilon_2]\Delta\theta, \tag{11}$$

and

$$\Delta\epsilon_2 = \tfrac{1}{2}[k(\epsilon_1-1)+n\epsilon_2](\Delta R/R)$$
$$-[n(\epsilon_1-1)-k\epsilon_2]\Delta\theta. \tag{12}$$

In Eq. (11) and Eq. (12) the index of refraction n, the extinction coefficient k, and the real and imaginary parts of the dielectric constant have their usual definitions and are interrelated as follows:

$$\epsilon_1 = n^2 - k^2, \tag{13}$$

$$\epsilon_2 = 2nk. \tag{14}$$

The reflectivity R is given by the Fresnel equation for normal incidence

$$R = \left|\frac{n-ik-1}{n-ik+1}\right|^2. \tag{15}$$

Figures 2 and 3 show the coefficients of the $\Delta R/R$ and of the $\Delta\theta$ term in Eq. (12) for copper, silver, and gold as calculated from the values of the optical constants given by Schulz,[24] by Ehrenreich and Philipp,[25] and by Cooper et al.[26] It is noteworthy that for photon energies above approximately 2.4 eV the contribution of $\Delta\theta$ to $\Delta\epsilon_2$ for the cases of Cu and Au far outweighs that of $\Delta R/R$. For silver the contributions of $\Delta R/R$ and $\Delta\theta$ are comparable in magnitude above ~3.6 eV. Since it is $\Delta\epsilon_2$ that is most directly related to any changes in critical points in the joint density of states and to changes in optical matrix elements, a direct

[23] T. S. Moss, S. D. Smith, and T. D. F. Hawkins, Proc. Phys. Soc. (London) **B70**, 768 (1962); F. C. Jahoda, Phys. Rev. **107**, 1261 (1957); H. R. Philipp and E. A. Taft, *ibid.* **113**, 1002 (1959).

[24] L. G. Schulz, J. Opt. Soc. Am. **44**, 357 (1954); L. G. Schulz and F. R. Tangherlini, *ibid.* **44**, 362 (1954).

[25] H. Ehrenreich and H. R. Philipp, Phys. Rev. **128**, 1622 (1962).

[26] B. R. Cooper, H. Ehrenreich, and H. R. Philipp, Phys. Rev. **138**, A494 (1965).
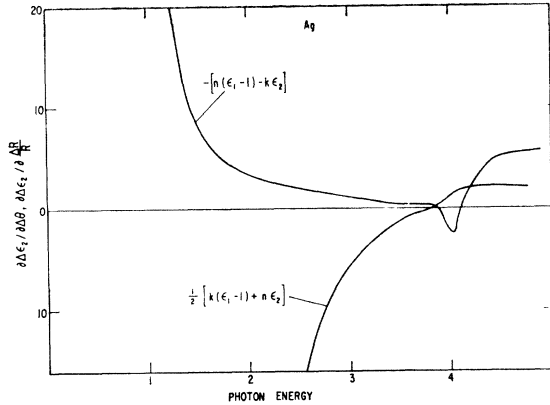
FIG. 3. The coefficients multiplying $\Delta R/R$ and $\Delta\theta$ in Eq. (4) evaluated for silver. The quantity $-[n(\epsilon_1-1)-k\epsilon_2]$ multiplies $\Delta\theta$ and $\frac{1}{2}[k(\epsilon_1-1)+n\epsilon_2]$ multiplies $\Delta R/R$.

interpretation of structure in $\Delta R/R$ at a particular wavelength in terms of transitions between electronic states with the corresponding energy difference may lead to misleading results.

In order to use Eq. (10), it is necessary to extrapolate the data to higher and lower energies. At low energies the optical constants of metals are dominated by the free-carrier absorption due to the conduction electrons. This absorption is characterized by a lifetime τ and a plasma frequency $\omega_p = (4\pi ne^2/m^*)^{1/2}$. Thus, at energies well below the onset of interband transitions, we have

$$\epsilon_2 = \epsilon_{2\text{ free carrier}} = \frac{\omega_p^2 \tau}{\omega(1+\omega^2\tau^2)}. \tag{16}$$

Changes in the free carrier ϵ_2 arise through variation of both τ and ω_p. Straightforward differentiation of Eq. (16) yields

$$\frac{\Delta\epsilon_2}{\epsilon_2} = 2\frac{\Delta\omega_p}{\omega_p} + \left(\frac{1-\omega^2\tau^2}{1+\omega^2\tau^2}\right)\frac{\Delta\tau}{\tau}. \tag{17}$$

Assuming that the effective mass m^* is independent of strain and that only the volume change $\Delta V/V$ contributes to changes in the plasma frequency, we obtain

$$\Delta\omega_p/\omega_p = -\tfrac{1}{2}\Delta V/V. \tag{18}$$

With the same assumptions, the value of $\Delta\tau$ may be obtained from the pressure variation of the resistivity. Differentiation of the expression for the bulk resistivity, $\rho^{-1} = ne^2\tau/m^*$, yields

$$\Delta\tau/\tau = \Delta V/V - \Delta\rho/\rho, \tag{19}$$

which may be rewritten in the form

$$\Delta\tau/\tau = (\tfrac{2}{3} - d\ln R/d\ln V)\Delta V/V. \tag{20}$$

Combining Eqs. (17) and (20), we obtain

$$\frac{\Delta\epsilon_2}{\epsilon_2} = \left\{-1 + \left(\frac{1-\omega^2\tau^2}{1+\omega^2\tau^2}\right)\left(\frac{2}{3} - \frac{d\ln R}{d\ln V}\right)\right\}\frac{\Delta V}{V}. \tag{21}$$

The experimental values for $\Delta V/V$, Lawson's[27] tabulated numbers for $d\ln R/d\ln V$ (5.1 for Au, 2.6 for Cu, and 3.6 for Ag), and the values for τ and ϵ_2 given by Ehrenreich and Philipp[25] and Cooper et al.[26] were used in Eq. (21) to calculate the free carrier $\Delta\epsilon_2$. The free-carrier contribution to $\Delta\epsilon_1$ may be similarly calculated and is given by

$$\Delta\epsilon_1/(\epsilon_1-1) = 2\Delta\omega_p/\omega_p = -\Delta V/V. \tag{22}$$

Unlike $\Delta\epsilon_2$ some contribution to $\Delta\epsilon_1$ due to the interband transitions will be present even for energies well below the onset of these transitions. At a sufficiently low energy, however, this term may be neglected in comparison to the free-carrier term of Eq. (22). By inverting Eqs. (11) and (12), the values of $\Delta R/R$ and $\Delta\theta$ predicted by the free-carrier model may be calculated. These calculated values of $\Delta R/R$ may be used to extrapolate the measured values of $\Delta R/R$ to low energies. In general, the zero level of the measured $\Delta R/R$ curves must be adjusted so that the two regions join smoothly. Values of $\Delta\theta$ at low energies can then be calculated by means of Eq. (10). It is convenient to divide the range of integration into three regions. These are the low-energy free-carrier range, the range of measured values, and finally all higher energies. Values of $\Delta R/R$ in the first range were obtained by the free-carrier extrapolation as described above and in the second range by actual measurement. Differences between values of $\Delta\theta$ calculated from the integral of Eq. (10) extended over these first two regions and those obtained from the free-carrier model are presumably due to having omitted the high-energy range. Values of $\Delta R/R$ at a selected set of points in this range may be uniquely determined by requiring that the Kramers-Kronig integral over this third region yield this dif-
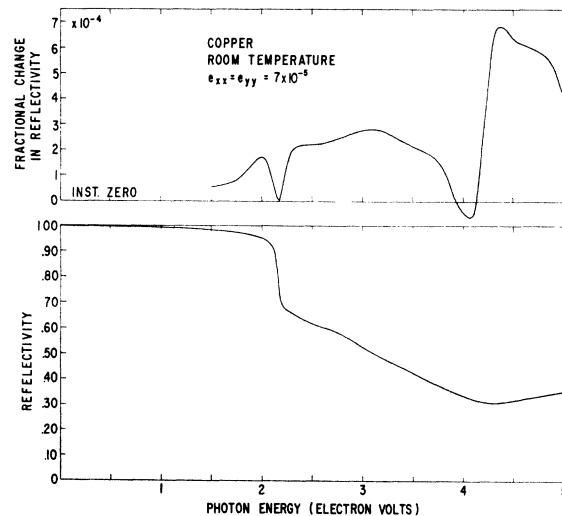
FIG. 4. The experimentally observed values of $\Delta R/R$ for copper as compared with the reflectivity values themselves. The convention adopted is that positive ΔR corresponds to dilatation.
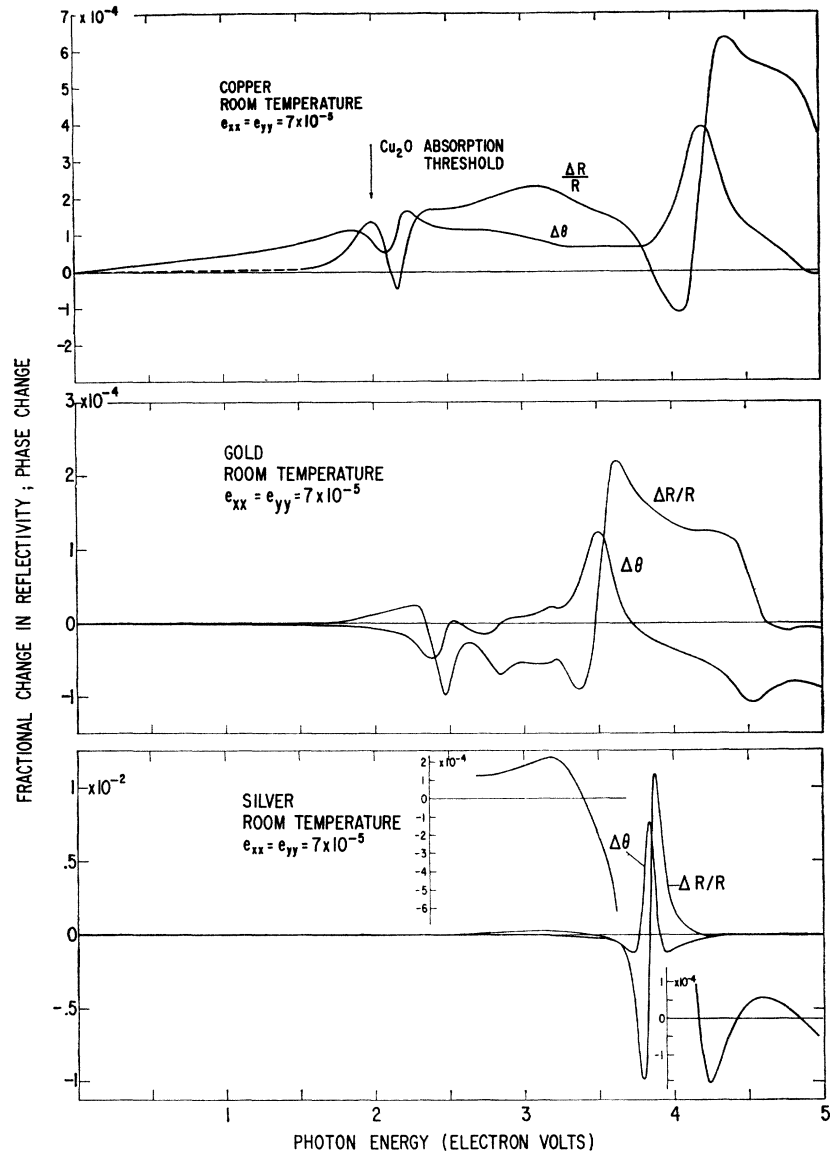
FIG. 5. $\Delta R/R$ for copper, silver, and gold adjusted and extrapolated as described in the text. The $\Delta\theta$ shown is obtained from $\Delta R/R$ by a Kramers-Kronig inversion. The results for silver are expanded in the insets to show the structure that is otherwise masked by the exceedingly strong structure centered at 3.84 eV.

ference in $\Delta\theta$ at a corresponding number of points in the free-carrier range. To some extent, then, one can determine the way the data should be extrapolated to higher energy by requiring that the resulting $\Delta\theta$ agree with the free-carrier model at low energy.

V. RESULTS AND DISCUSSION

The directly measured experimental results for copper are shown in the upper part of Fig. 4. The lower curve shows for comparison the reflectivity values of Ehren-reich and Philipp in the same energy range. Although, as expected, the positions of the structure in $\Delta R/R$ are correlated with those in the reflectivity, ΔR is obviously not simply the derivative of the reflectivity curve. Figure 5 shows the values of $\Delta R/R$ for Cu, Ag, and Au when adjusted to match the free-carrier model as de-

scribed above. Also shown are the $\Delta\theta$ as obtained from the Kramers-Kronig inversion, Eq. (10). The zero offset of the experimental $\Delta R/R$ values amounted to 5.1×10^{-5}, 2.2×10^{-5}, and 4.7×10^{-5} for copper, silver, and gold, respectively. The strain-induced changes in the dielectric constant, $\Delta\epsilon_1$ and $\Delta\epsilon_2$, as obtained from $\Delta R/R$ and $\Delta\theta$ using Eqs. (11) and (12), are shown in the bottom halves of Figs. 6, 7, and 8. The values of $\Delta\epsilon_2$ calculated from the volume variation of the free-electron model are shown as the full dots at the low-energy end of the curves for $\Delta\epsilon_2$. The values of $\Delta\epsilon_1$ calculated in the same manner are shown as open circles. The procedure outlined above was used to fit the calculated curves to these points for both silver and gold. In the case of copper, however, the procedure could not be applied without the introduction of unreasonably large oscillators in the
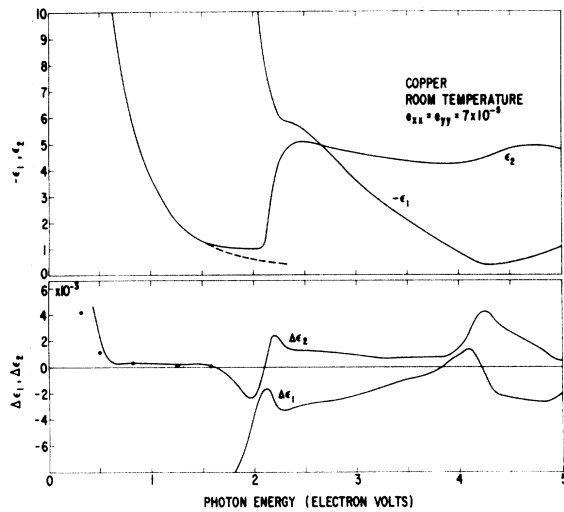
FIG. 6. $\Delta\epsilon_1$ and $\Delta\epsilon_2$ for copper obtained by means of Eqs. (11) and (12) and the procedure described in the text. The solid circles are the values of $\Delta\epsilon_2$ that are obtained from the free-electron model. It was not possible to fit $\Delta\epsilon_1$ to the free-carrier model for reasons described in the text. Values for ϵ_2 are shown in the upper half of the figure. The dashed curve is the extrapolated free-carrier behavior.

high-energy range. This problem most probably is caused by the oxidation of the copper surface. As was mentioned previously, the air oxidation of the copper sample causes a 50% change in the structure observed in the vicinity of 2 V. This is quite reasonable, since copper oxide has an absorption threshold starting at 2 V. Because of this factor, the copper data should be considered with some caution. The gross features of differential reflectivity spectra, however, are relatively
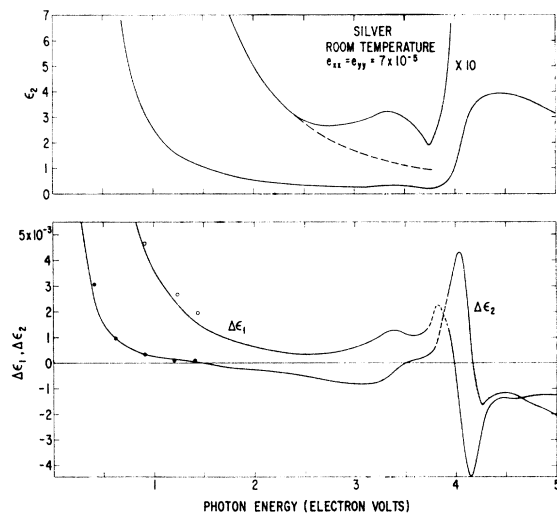
FIG. 7. $\Delta\epsilon_1$ and $\Delta\epsilon_2$ for silver obtained by means of Eqs. (11) and (12) and the procedure described in the text. The solid circles are the values of $\Delta\epsilon_1$ and the open circles are the $\Delta\epsilon_1$ that are obtained from the free-electron model. Values for ϵ_2 are shown in the upper half of the figure. The dashed curve is the extrapolated free-carrier behavior.

unaffected by these factors, and for that reason the data are presented. High-vacuum measurements on freshly evaporated copper films would avoid this problem.

The $\Delta\epsilon_1$ and $\Delta\epsilon_2$ result partly from the dilatation and are in part due to shear effects averaged over the various crystallographic orientations of the film crystallites. As discussed above, measurements made upon single crystals using polarized light are necessary to unambiguously separate out the various contributions.

A comparison of the curves for $\Delta\epsilon_2$ with the $\Delta R/R$ results of Fig. 5 shows the value of the Kramers-Kronig inversion and the virtue of presenting the measure-
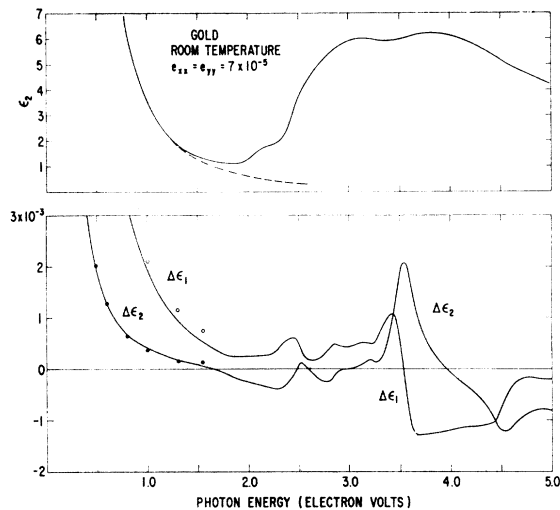
FIG. 8. $\Delta\epsilon_1$ and $\Delta\epsilon_2$ for gold obtained by means of Eqs. (11) and (12) and the procedure described in the text. The solid circles are the values of $\Delta\epsilon_2$ and the open circles are the $\Delta\epsilon_1$ that are obtained from the free-electron model. Values for ϵ_2 are shown in the upper half of the figure. The dashed curve is the extrapolated free-carrier behavior.

ments in terms of $\Delta\epsilon_1$ and $\Delta\epsilon_2$. The shapes of both $\Delta\epsilon_1$ and $\Delta\epsilon_2$ for all three metals are, as anticipated above, radically different from those of $\Delta R/R$ over the entire range. Since $\Delta\epsilon_2$ is most closely related to any physical model of the material, comparison of theory with experiment is most advantageously made with it rather than with $\Delta R/R$.

The $\Delta\epsilon_2$ curves for copper and gold are qualitatively quite similar in the energy range above the free-carrier region. The first structure to appear is a broad negative peak in $\Delta\epsilon_2$ followed immediately by a positive peak. There is then a region of relatively weak structure extending in the case of gold from 2.7–3.4 eV and in copper from 2.2–4.0 eV. Major structure again appears at high energy as a positive peak followed by a well-separated negative peak. In gold these higher energy peaks are at 3.5 and 4.5 eV, respectively, and in copper they appear at 4.2 and 5.0 eV. The structure in $\Delta\epsilon_2$ can be understood by considering the origin of e_2 and the manner in which the quantities appearing in the expression for e_2 will vary under strain. The quantity

ϵ_2 is given by

$$\epsilon_2 = A |M|^2 \rho_{ul}, \tag{23}$$

where A is a constant, M is the interband matrix element which is a slowly varying function of energy, and ρ_{ul} is the joint density of states for interband transitions. Both M and ρ_{ul} depend on strain, but the most profound change is due to the relative motion of a given pair of bands. This gives rise to a strain-induced change in the onset energy for a particular transition. To a first approximation the change in ϵ_2 arising from this cause is

$$\Delta\epsilon_2 = (1/h)(\partial\epsilon_2/\partial\omega)\Delta E_b, \tag{24}$$

where ΔE_b is the strain-induced relative shift of the two bands contributing to ϵ_2. In the vicinity of either Van Hove[28] or Fermi surface singularities[25] in the joint density of states, Eq. (24) predicts a peak in $\Delta\epsilon_2$. At photon energies higher than the very first interband transitions the situation is more complex because of contributions to ϵ_2 by more than just one pair of bands. In this case, ϵ_2 is given by

$$\Delta\epsilon_2(\omega)^{\text{total}} = \sum_i \epsilon_2{}^i(\omega) \tag{25}$$

and Eq. (24) becomes

$$\Delta\epsilon_2(\omega)^{\text{total}} = \frac{1}{h} \sum_i \frac{\partial\epsilon_2{}^i(\omega)}{\partial\omega} \Delta E_b, \tag{26}$$

where the sums in Eqs. (25) and (26) are over all pairs of bands which contribute to ϵ_2 at ω. Under these circumstances, a singularity in the joint density of states between two bands at an energy difference corresponding to a photon energy of $h\omega$ still produces a local maximum in $\Delta\epsilon_2$ at ω. It is, however, superimposed upon a background consisting of the contributions from all other bands. Therefore, although the location in energy of a peak in $\Delta\epsilon_2$ indicates the existence of a critical point at the corresponding energy difference, the magnitude of the peak in $\Delta\epsilon_2$ cannot be used to calculate a deformation potential unless the background $\Delta\epsilon_2$ is subtracted.

An observation of the data causes us to conclude that there are critical points in the joint densities of states of Cu at 4.2 and 5.0 eV and in that of Au at 3.5 and 4.5 eV. As may be seen from the upper halves of Figs. 6 and 8, these results are consistent with the structure observed in ϵ_2 of Cu and Au as reported by Schulz, Ehrenreich and Philipp, and Cooper et al. These high-energy peaks occur at almost precisely those energies for which the ϵ_2 curves themselves have local maxima or minima in their slopes. Ehrenreich and Philipp and Cooper have, on the basis of Segall's[29] band structure calculations, tentatively assigned the lower of these

[27] A. W. Lawson, Progr. Metal Phys. **6**, 1 (1956).
[28] L. Van Hove, Phys. Rev. **89**, 1189 (1953).
[29] B. Segall, Phys. Rev. **125**, 109 (1962).

FIG. 9. The shape of $\omega^2\epsilon_2$ and $\Delta\epsilon_2$ for the d-band-to-Fermi-surface transition for the case where the joint density of states increases with increasing photon energy. The curves marked "positive" and "negative" refer to strain-induced increases and decreases, respectively, in the d-band-to-L_2' energy difference.
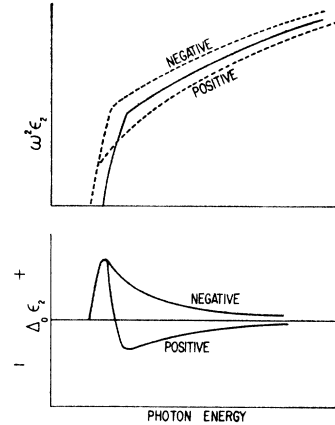
singular points to transitions from $X_5 \to X_{4'}$ and the higher to transitions from $L_{2'} \to L_{12}$. Piezoreflection experiments made with polarized light upon single crystals are needed to unambiguously assign these transitions.

The positive structure in $\Delta\epsilon_2$ beginning at 2.1 eV for copper and 2.4 eV for gold and the immediately following weak structure occur at the same energy as do the first sharp rise in ϵ_2 for these metals. This structure may be qualitatively understood on the basis of a deformation potential model. The rise in ϵ_2 at these energies has been discussed in considerable detail by Ehrenreich and Philipp[25] and Cooper et al.[26] who attribute it to the onset of d-band-to-Fermi-surface transitions near L and consider these transitions to be the lowest energy interband transitions. The contribution to ϵ_2 due to these transitions is affected by strain in two ways. First, the $L_{32}-L_{2'}$ d-band-to-conduction-band energy difference will be changed, and second, the location of the Fermi energy relative to the bottom of the conduction band at Γ_1 will also be changed. The nature of the contributions that each of these changes makes to $\Delta\epsilon_2$ may be understood by considering Figs. 9 and 10.

The solid curve in the upper half of these figures shows the two possible shapes of $\omega^2\epsilon_2$ for d-band-to-Fermi-surface transitions. The quantity $\omega^2\epsilon_2$, which for photon energies greater than the d-band–Fermi-surface separation is proportional to the joint density of states for vertical transitions, increases in the case of Fig. 9 and decreases for Fig. 10. The initial rapid rise in both is due, in large measure, to the flatness of the low-lying L_{32} d band. This makes the contours of constant energy difference between it and the conduction band practically coincide with the surfaces of constant energy for electrons in the conduction band. Therefore, as soon as the incident photon energy reaches a threshold which is given by

$$E_T = E_F - E_d, \tag{27}$$

where E_d is the energy of the flat d band and E_F is the Fermi energy, a large number of interband transitions become possible within a narrow energy range.

This effect gives rise to the initial sharp rise in ϵ_2 in Figs. 9 and 10. Although, in general, changes in E_T arise from both terms in Eq. (27), the location of the d band should be essentially unchanged by dilatation. The change in the threshold energy is thus due only to the change in Fermi energy,

$$\Delta E_F = -\tfrac{2}{3}E_F\Delta V/V + \Delta E(\Gamma_1). \tag{28}$$

If one assumes that the motion of the minimum of conduction band at Γ_1 is either small or negative, the threshold energy is shifted to lower energy independent of whether the density of states at the Fermi surface increases or decreases. In addition, the joint density of states will be shifted to either higher or lower energy according to whether the deformation potential of the p-like part of the conduction band near $L_{2'}$ is either positive or negative.

The resulting $\omega^2\epsilon_2$ curves for the strained material are shown as the dashed curves marked "positive" and "negative" in Figs. 9 and 10. A simple subtraction and division by ω^2 gives the shapes of $\Delta\epsilon_2$ which are shown in the lower halves of Figs. 9 and 10. A comparison of the shapes of these curves with the observed $\Delta\epsilon_2$ for copper and gold indicates that either (a) the density of states increases and the $L_{2'}$ deformation potential is negative, or (b) the density of states decreases and the deformation potential is positive. The joint density of states as calculated by Cooper *et al.* for Cu and Au decreases as the energy increases, so presumably, the $L_{2'}$ deformation potential is positive. This behavior is opposite to that obtained by Ham[30] in his calculation of the band structure for the alkali metals. In the course of this calculation he investigated the effects of varying the lattice parameter. His results indicate that the energies at all symmetry points possessing d-like character are essentially independent of lattice parameter, while the energies of all s- and p-like eigenstates at symmetry points decrease as the lattice parameter in-
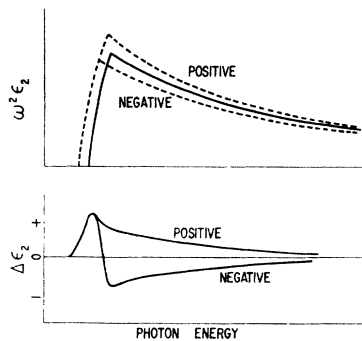
Fig. 10. The shape of $\omega^2\epsilon_2$ and $\Delta\epsilon_2$ for the d-band-to-Fermi-surface transitions for the case where the joint density of states decreases with increasing photon energy. The curves marked "positive" and "negative" refer to strain-induced increases and decreases respectively in the d-band-to-$L_{2'}$ energy difference.

[30] F. Ham, Phys. Rev. **128**, 82 (1962).
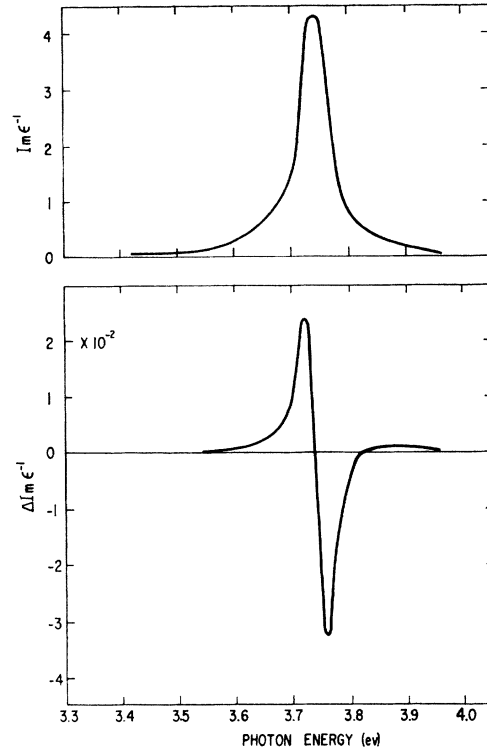
Fig. 11. The energy loss term for silver and the corresponding strain-induced changes in the vicinity of the sharp reflectivity minimum.

creases. His results indicate further that the volume deformation potential of the Γ_1 minimum is approximately $+1$ eV for all of the alkali metals. This, together with the fact that E_F for the noble metals is 9 eV, makes reasonable our assumption that ΔE_F is negative.

The experimental results for silver are dominated by a derivative-like structure in $\Delta R/R$ centered at 3.83 eV whose peak-to-peak amplitude, 2×10^{-2}, is more than twenty times greater than anything observed for either copper or gold. This structure in $\Delta R/R$ occurs at precisely the same energy as does the sharp and narrow minimum in R[31] and is obviously connected to it. Ehrenreich and Philipp have explained this sharp reflectivity minimum in terms of a hybrid plasma resonance arising from interactions between the conduction and the d-electrons. They made clear the plasma-resonance-like character of the optical properties of silver in this vicinity by showing that the energy loss function, $\mathrm{Im}\ \epsilon^{-1} = \epsilon_2/(\epsilon_1^2 + \epsilon_2^2)$, is sharply peaked there while both ϵ_1 and ϵ_2 are quite small. This behavior of $\mathrm{Im}\ \epsilon^{-1}$ is shown in the upper half of Fig. 11. The strain-induced changes in $\mathrm{Im}\ \epsilon^{-1}$ are given by

$$\Delta\,\mathrm{Im}\epsilon^{-1} = \frac{(\epsilon_1^2 - \epsilon_2^2)\Delta\epsilon_2 - 2\epsilon_1\epsilon_1\Delta\epsilon_1}{(\epsilon_1^2 + \epsilon_2^2)^2}, \tag{29}$$

[31] E. A. Taft and H. R. Philipp, Phys. Rev. **121**, 1100 (1961).

which is shown plotted in the lower half of Fig. 11. The values used to obtain Fig. 11 are our results for $\Delta\epsilon_1$ and $\Delta\epsilon_2$ and those of Ehrenreich and Philipp for ϵ_1 and ϵ_2. Figure 11 shows that $\Delta \text{Im}\epsilon^{-1}$ has a derivative-like shape when compared with the energy loss function itself. This results from the change in sign of ϵ_1 in the second term of Eq. (29) when ϵ_1 crosses zero. This result and the sign of the derivative may be explained qualitatively by a rigid band deformation potential model whose net effect is to shift the location of the hybrid plasma resonance to lower energy. Since ϵ_1 is the sum of two terms, a free-carrier term ϵ_1' and an interband term ϵ_1^b, changes in both contribute to the shift of the zero crossing. The effect of dilatation upon the free carrier ϵ_1 is according to Eq. (22) a shift of ϵ_1 to lower energy. It is not possible in a similarly *a priori* manner to calculate the sign of the shift due to the interband contributions to $\Delta\epsilon_1$. If, however, as in the cases of Cu and Au, the lowest energy interband transitions are d-band-to-Fermi-surface transitions, the sign of the shift in ϵ_1^b may also be obtained.

The position in energy of ϵ_1^b in this case is determined by the threshold given in Eq. (27). As above, one expects ΔE_d to be small, with the result that the changes in Fermi energy determine $\Delta\epsilon_1^b$. By the arguments given above, ΔE_F is negative for dilatation. Thus, contributions to ϵ_1 from both the free electron and the interband terms predict the same sign for the derivative as that observed.

It is noteworthy that although the major structure in $\Delta R/R$ for silver is, as was mentioned, 20 times larger than that for Cu or Au, the changes in the dielectric constants, $\Delta\epsilon_1$ and $\Delta\epsilon_2$ for Cu, Ag, and Au are all of the same scale. The strong structure in $\Delta R/R$ does not produce correspondingly strong structure in $\Delta\epsilon_2$. However, since $\Delta R/R$ and $\Delta\theta$ are both varying quite rapidly near 3.8 eV, $\Delta\epsilon_1$ and $\Delta\epsilon_2$ as calculated from Eqs. (11) and (12) are very sensitive to the precise values of ϵ_1 and ϵ_2 in that region. The $\Delta\epsilon_1$ and $\Delta\epsilon_2$ curves in Fig. 7 are therefore shown dashed in the region immediately adjacent to 3.84 eV. Under the assumption that the sharp rise in ϵ_2 for silver in the vicinity of 4 eV is caused by the onset of d-band-to-Fermi-surface transitions, this structure may be qualitatively understood on the basis of the same deformation potential model as was previously applied to the d-band–Fermi-surface transitions in Cu and Au. For the case of silver, however, the initial strong positive peak in $\Delta\epsilon_2$ is immediately followed by a strong negative peak. The joint density to states for silver, as calculated by Cooper *et al.*, decreases as does that for Cu and Au. Therefore, in this case, in order to obtain the observed structure in $\Delta\epsilon_2$ the conduction-band–d-band net deformation potential must be negative. As before, dilatation causes the Fermi surface to shift to lower energy making, thereby, positive contributions to $\Delta\epsilon_2$. The negative band deformation potential shifts the higher energy

interband ϵ_2 to lower energies, thus producing negative values of $\Delta\epsilon_2$. The net result of these two processes is shown as the $\Delta\epsilon_2$ curve marked "negative" in Fig. 10.

At lower energies, the $\Delta\epsilon_2$ results are to some extent inconsistent with earlier conclusions about the threshold energy for interband transitions. Both Cu and Au exhibit broad negative structure in $\Delta\epsilon_2$ which extends down to 1.5 eV. This negative structure begins at 2.1 eV in Cu and 2.4 eV in Au and is peaked at 1.95 and 2.30 eV in copper and gold, respectively. The thresholds for the d-band-to-Fermi-surface transitions, considered by Cooper *et al.* to be the first interband transitions, are 2.09 and 2.35 eV for Cu and Au, respectively. Therefore, essentially all of this negative structure in $\Delta\epsilon_2$ occurs in a region of the spectrum hitherto considered to be below the onset of interband transitions. The data for silver shown in Fig. 7 exhibit the same negative $\Delta\epsilon_2$ at photon energies below 3.4 V extending down to approximately 2.0 eV. The onset of interband transitions in this case has been given as 3.97 eV so silver too exhibits structure in $\Delta\epsilon_2$ at photon energies below what has been considered to be the threshold for interband transitions. Our observations suggested a careful re-examination of the ϵ_2 data for Cu, Ag, and Au for energies below 2.09, 3.97, and 2.35 eV, respectively. As may be seen in Figs. 6, 7, and 8 there are in fact small but significant departures of the data from the ϵ_2 values obtained by extrapolation of the free-carrier results at low energies. These departures occur in exactly the same energy regions as the negative structure observed in $\Delta\epsilon_2$. This departure is largest for gold where the additional ϵ_2 has a peak value of ~ 1.3 at 2.2 eV. The copper results also deviate from the extrapolated free-carrier ϵ_2 and the data for silver actually exhibit a well-defined peak at 3.4 eV whose amplitude is $\simeq 0.2$. This peak in ϵ_2 for silver appears to be correlated with a weak peak in $\Delta\epsilon_2$. An exact free-carrier extrapolation is impossible because of the energy dependence of τ in Eq. (16) which shows up experimentally as a departure of ϵ_2 from a simple ω^{-3} dependence. The extrapolation procedure followed was simply to extrapolate the free-carrier ϵ_2 according to the low-energy experimentally observed ω^{-n} dependence. The structure in ϵ_2 and the accompanying structure in $\Delta\epsilon_2$ may be explained by either a strong frequency and strain dependence of τ or by interband transitions at lower energies than previously considered. The first possibility would appear to be unreasonable in view of the relatively strong structure observed in ϵ_2. This question, however, must remain open until a theory for the strong variation of τ with frequency and strain is presented, or until the interband transitions involved are identified. The $\Delta\epsilon_2$ due to these "extra" transitions has approximately the same amplitude as that arising from the "usual" interband transitions whereas the corresponding ϵ_2 is much smaller. These transitions

must, therefore, be much more strain-dependent than the higher energy transitions.

The anomalies in $\Delta\epsilon_2$ just described are qualitatively quite different from those observed by El Naby and Mayer[32] in potassium. The piezoreflection data show additional absorption at the high-energy end of the free-carrier region which appears as a precursor to the usual interband transitions. These observations correlate with weak *positive* contributions to ϵ_2. El Naby and Mayer,[15] on the other hand, observe deviations from the free-electron behavior at long wavelengths. Their measured ϵ_2 falls *below* the free-electron extrapolation at wavelengths longer than approximately 1.5 μ.

Note added in proof.—The noble metal anomalies, however, bear some resemblance to low energy peaks in the optical constants of Na, Rb, and Li recently reported by Mayer and by Hodgson in the *Proceedings of the International Colloquium on Optical Properties and Electronic Structure of Metals and Alloys* (North Holland Publishing Company, Amsterdam, 1966). Mayer presented data for Na and Rb which exhibit peaks in $\omega\epsilon_2$ at 1.7 and 1.0 eV, respectively, falling in both cases at the high energy end of the Drude absorption, yet well below the onset of well defined interband transitions. The peak in sodium had also been previously reported by Hodgson, J. Phys. Chem. Solids **24**, 1213 (1963). Similarly, Hodgson's data for Lithium show a peak in $\omega\epsilon_2$ at 2.8 eV, again below the experimentally observed threshold for interband transitions at 3.2 eV. While further experimental work is clearly needed, it appears as if similar anomalies in ϵ_2 occur for both the noble and the alkali metals. This suggests the possibility that the causes for the anomalies are not unique to either but are of more general origin.

VI. SUMMARY AND CONCLUSIONS

It has been shown in this paper that the measurement of the differential piezoreflectance effect can yield information about the band structure of solids. The raw data in many instances display sharp structure which, if sufficiently detailed band structure calculations exist,

can be directly correlated with expected critical points. Since the structure is generally much sharper than that seen in reflectance or transmission, this experiment can be more precise. The raw data, however, do not correspond directly to the interband transitions, and in many instances the structure seen in $\Delta R/R$ can be misleading.

A procedure for obtaining the strain-induced changes in the dielectric constant from the piezoreflectance data has therefore been presented. When the data are analyzed in this manner, new information can be obtained and the location of the various critical points in the B.Z. can be deduced. Thus, it may not be necessary to have an accurate, first principles band structure calculation before some features of the band structure of the sample can be classified. The increased sensitivity of this experiment makes it possible to discern features that may have been beyond the reach of other experiments. Furthermore, the deformation potentials of the bands involved in the interband transitions may be deduced.

The experimental results for the noble metals confirm that critical points are located at energies previously identified. The assignments of these points to specific transitions was not confirmed, however, because the required set of experiments on single-crystal specimens was not done. The over-all structure was in qualitative agreement with the deformation-potential model, and on this basis the signs of the deformation potentials of some of the transitions were tentatively assigned. The results for all three metals show additional structure in a region lower in energy than that for which structure has been previously detected. The most reasonable explanation for this is that there are interband transitions possible at lower energy than has previously been presumed. The similarity in the character of the resulting structure in $\Delta\epsilon_2$ indicates that the same transitions are involved for copper, silver, and gold.

[32] H. Mayer and M. H. El Naby, Z. Physik **174**, 289 (1963).